Available online at www.sciencedirect.com
ScienceDirect
Ceramics International 35 (2009) 2999–3004
CERAMICS INTERNATIONAL
www.elsevier.com/locate/ceramint

Effects of zinc oxide on thermal shock behavior of zinc sulfide–silicon dioxide ceramics

J.K. Chen [a,*], K.L. Tang [a], J.T. Chang [b]

[a] Department of Materials and Mineral Resources Engineering, National Taipei University of Technology, No.1, Sec.3, Zhong-Xiao E. Rd., Taipei 10608, Taiwan, ROC
[b] Non-Ferrous Product Development Section, Steel and Aluminum Research & Development Department, China Steel Corporation, Kaohsiung 81233, Taiwan, ROC

Received 15 October 2008; received in revised form 13 March 2009; accepted 2 April 2009
Available online 24 April 2009

Abstract

Thermal shock resistances of ZnO and non-ZnO containing ZnS–SiO_2 composite ceramics are observed using water quenching method. The residual strengths are measured as function of quenching temperature differences. The thermal shock damage parameters R''' and R'''' are evaluated to compare with experimental results. Specimens with low thermal shock damage parameters show acute strength degradation up to 76% at a lower quenching temperature difference of 250 °C. The 1% ZnO containing specimen with medium density and higher thermal shock damage parameter values demonstrates a minimal strength drop of 36% at a higher quenching temperature difference of 300 °C. The evaluated R''' and R'''' values correspond well with the residual strength at elevated temperature difference. It implies that the good thermal shock resistance of ZnS–SiO_2 system can be achieved by improving fracture toughness with moderate ZnO addition and pores.

Keywords: Thermal shock resistance; ZnS–SiO_2; Composite ceramic; Thermal shock damage parameters

1. Introduction

Zinc sulfide–silicon dioxide (ZnS–SiO_2) composite ceramics are widely utilized as dielectric protection films in phase change optical media [1,2] due to their good thermal stability and moderate thermal conductivity [3]. RF magnetron sputtering process is usually applied to make optical thin films from bulk ZnS–SiO_2 sputtering targets. These composite ceramic targets are often damaged during sputtering process. The target fracture is mainly caused by the great temperature difference between sputtering and cooling surfaces of the sputtering targets. Therefore, this study will concentrate on the thermal shock resistance properties of these materials. The objectives of this study are to understand the controlling factors of thermal shock behaviors in these materials and find ways to improve their thermal shock resistance properties.

Thermal shock property measurements of ceramic materials have been standardized by quenching specimens from different heating temperatures into a chosen cooling medium, such as room temperature water or oil. A variety of thermal and mechanical responses are measured under the effects of different quenching temperatures [4]. Several theories are proposed to explain the behaviors of ceramic materials in these thermal shock experiments.

Research on thermal shock of ceramic material begins back in 1950s. The unified thermal shock resistance theory is proposed by Hasselman [5–8] and some other affecting factors are reported by Kingery [9]. On the basis of thermal shock resistance theory, two groups of parameters are developed to predict the thermal shock behaviors of ceramic materials. One group consists of thermal shock fracture (TSF) parameters and the other consists of thermal shock damage (TSD) parameters. The TSF parameters [10,11] focus on the resistance to crack initiation due to thermal stresses. These are especially suited for applications in idealized brittle materials without micro-pores or micro-cracks.

The TSD parameters focus on crack propagation and extension resistance stages during thermal shock of ceramic materials [10,11]. These parameters are particularly useful in evaluating thermal shock properties of ceramics containing

* Corresponding author. Tel.: +886 2 27712171x2763; fax: +886 2 27317185.
E-mail address: jkchen@ntut.edu.tw (J.K. Chen).

0272-8842/$36.00
doi:10.1016/j.ceramint.2009.04.006

micro-pores and micro-cracks. In current study, the porosity of ZnS–SiO_2 composite ceramics is up to 17%, therefore TSD parameters are selected to discuss their thermal shock behaviors.

The fracture strength and fracture toughness [12] are measured to evaluate the TSD parameters of ZnS–SiO_2 with varied sintering density and ZnO concentrations. The relations of TSD parameters with actual thermal shock fracture behaviors are observed and discussed.

2. Experimental procedure

80 mol% ZnS (99.99% purity) and 20 mol% SiO_2 (99.99% purity) powders are weighed for preparing non-ZnO containing specimens. The powders are ball milled to ensure a uniform mixture. Non-ZnO containing specimens are hot pressed under 10^{-3} Torr vacuum at 1060 °C and a uniaxial pressure of 30 or 46 MPa for two hours. The two different pressures are used to obtain specimens with low or high densities, respectively.

1 wt% and 3 wt% ZnO (99.99% purity) are mixed into 80 mol% ZnS–20 mol% SiO_2 mixtures to produce ZnO containing specimens. Two ZnO containing specimens are hot pressed using the same 10^{-3} Torr vacuum and 1060 °C temperature while fixing the pressure at 46 MPa to compare the effects of different ZnO concentrations.

Bulk densities of sintered specimens are measured using Archimede's method with deionized water as medium. The relative density is defined as the measured density divided by the theoretical density. The theoretical density is estimated using rule of mixtures by all major components ($\rho_{ZnS} = 4.09\ g\ cm^{-3}$, $\rho_{SiO_2} = 2.196\ g\ cm^{-3}$, and $\rho_{ZnO} = 5.6\ g\ cm^{-3}$) [13] assuming none or few reaction occurs among them. Phase analyses are conducted by X-ray diffraction (XRD) with Cu Kα radiation at a scan rate of 2°/min between 20° and 80°. Fractography for all specimens are observed using a Hitachi S-4700 field emission scanning electron microscope (SEM).

Thermal shock tests follow ASTM #C1525-04 standard [14]. The specimens are cut from as-sintered ceramics using diamond saw into dimensions of 6 mm × 6 mm × 55 mm. Their surfaces are ground and polished to eliminate surface defects. The specimens are heated at a rate of 5 °C/min to the preset temperatures and held for 15 min before quenching into 20 °C water bath. The quenched specimens are dried afterward at 100 °C for two hours to remove the moisture.

The retained flexural strengths (σ_f) are measured via four-point bending tests at a crosshead speed of 3.0 mm/min. The outer and inner spans of specimens are 30.0 mm and 10.0 mm, respectively. At least three bending tests are performed for each quenching temperature condition to obtain average residual strength. Hardness of each specimen is measured by micro-hardness tester using 2.4 N load for 20 s. Fracture toughness of specimens is determined by indentation method [15–17] using 9.8 N load for 20 s and Eq. (1) [18]. Three indentations are made to obtain a mean value of fracture toughness.

$$K_{IC} = 0.203\left(\frac{c}{a}\right)^{-3/2} H_v a^{1/2}. \quad (1)$$

where H_v is the Vickers hardness, a is the impression radius and c is the radial/median crack length.

3. Results and discussion

3.1. Phase identification

From XRD spectra shown in Fig. 1, there is a significant difference in the structures of ZnS. In samples without ZnO addition, ZnS bears sphalerite or low temperature structure which is stable at temperature lower than 1020 °C [19]. On the other hand, high temperature wurtzite structure is identified in ZnO containing specimens. Apparently, the high temperature wurtzite phase is stabilized by ZnO addition after cooling from 1060 °C hot pressing temperature. This can be explained by that ZnO also has wurtzite type structure [20].

In XRD analyses, willemite phase (Zn_2SiO_4) appears only in ZnO added specimens shown in Fig. 1. Willemite results from the reaction between ZnO and SiO_2 [21]. The original purpose of ZnO addition is to improve the sintering density by forming ZnO liquid phase [22]. However, densities of ZnO added specimens apparently do not improve as expected [23]. From XRD results, it is found that willemite instead of ZnO liquid phase forms due to the reaction between ZnO and SiO_2.

3.2. Indentation hardness and fracture toughness

Table 1 lists the mechanical properties of all specimens. Hardness of non-ZnO specimens is related to their flexural strengths and densities. Specimens with higher density also bear higher hardness and flexural strengths.

In all specimens tested, 3% ZnO added specimen demonstrates the highest hardness, although its density is not the highest. Formation of willemite at the ZnO and SiO_2 interfaces and wurtzite phase ZnS apparently contributes to the increase of hardness. Feldmann and co-worker [24] also report that addition of ZnO can improve the adhesion between SiO_2 and ZnS.

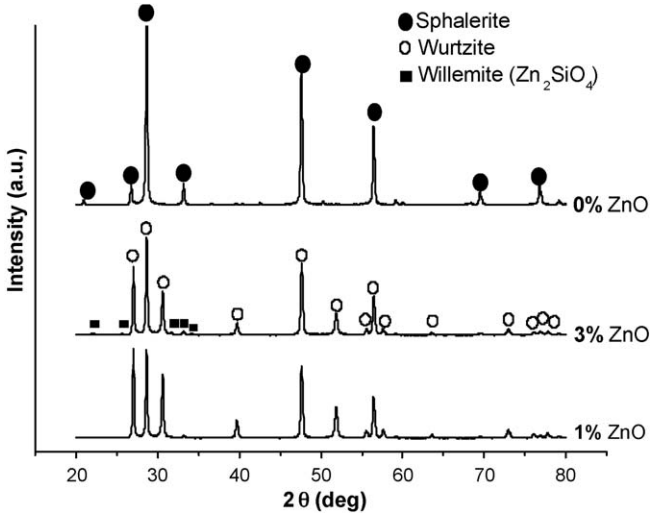

Fig. 1. XRD analyses of 0% ZnO and ZnO added specimens.

Table 1
Mechanical and thermal shock properties of 0% ZnO and ZnO added ZnS–SiO_2 composites.

wt% ZnO	0% ZnO	0% ZnO	1% ZnO	3% ZnO
Hot press pressure (MPa)	46	30	46	46
Relative density, ρ_{rel}	0.96	0.89	0.83	0.89
σ_f (MPa)	53.5 ± 5.02	36.8 ± 3.45	23.1 ± 2.25	33.8 ± 3.13
E (GPa)	91.25	91.25	91.49	91.98
ν	0.271	0.271	0.272	0.273
H_v (GPa)	2.25 ± 0.040	2.07 ± 0.082	1.53 ± 0.108	2.39 ± 0.020
K_{IC} (MPa $m^{1/2}$)	1.28 ± 0.023	1.23 ± 0.049	1.46 ± 0.103	0.8 ± 0.007
R''' (MPa^{-1})	43.7	92.4	235.5	110.7
R''''(μm)	785	1532	5487	771

Hardness of 1% ZnO added specimen is not as high as the 3% ZnO added specimen. The 1% ZnO addition causes the density to drop slightly [23], therefore the increase in hardness as a result of the improved interfacial effect is offset by the increased porosity.

The fracture toughness, K_{IC}, is defined as resistance to crack propagation and is obtained by indentation techniques. The highest fracture toughness is achieved by 1% ZnO added specimen (Table 1). Although the 3% ZnO specimen is also added with ZnO, it behaves relatively more brittle than other specimens, possibly due to its high density or excessive formation of willemite which will be discussed later.

The slightly higher porosity in 1% ZnO specimen not only reduces the fracture strength but also prevents the micro-cracks to extend by stress relief [25]. Therefore, it gives rise to a higher K_{IC}.

3.3. TSD parameters R''' and R''''

TSD parameters, R''' and R'''', are used as criteria to index the thermal shock resistance [10] in materials with micro-pores or micro-cracks. Since the materials reported in current study contain porosity as high as 17% (Table 1). TSD parameters are employed to evaluate thermal shock properties in current composite ceramic system. R''' and R'''' are expressed as follows [10]

$$R''' = \frac{E}{\sigma_f^2(1-\nu)} \tag{2}$$

$$R'''' = \frac{K_{IC}^2}{\sigma_f^2(1-\nu)} \tag{3}$$

where E is Young's modulus, σ_f is the flexural strength, ν is Poisson's ratio and K_{IC} is the fracture toughness. Assuming the effects of porosity on Young's moduli and Poisson's ratios are similar in all samples and are disregarded, E and ν can be evaluated directly by rule of mixture (4)–(6) [11]:

$$E = \sum_{i=1}^{3} E_i V_i \tag{4}$$

$$\nu = \sum_{i=1}^{3} \nu_i V_i \tag{5}$$

and

$$V_i = \frac{m_i/\rho_i}{\sum_i m_j/\rho_j} \tag{6}$$

where subscripts 1, 2 and 3 represent ZnS, SiO_2 and ZnO, respectively, and m_i and ρ_i are mass percentage and density of each composition. Young's moduli of ZnS, SiO_2 and ZnO used for estimation are 96.5, 72.95, and 128 GPa, respectively [26]. Poisson's ratios of ZnS, SiO_2 and ZnO are 0.3, 0.17, and 0.35, respectively [20]. Table 1 lists the mechanical properties of each specimen along with the calculated R''' and R'''' values.

In Table 1, 1% ZnO added specimen has the highest R''' and R'''' values of 235.5 MPa^{-1} and 5487 μm. The high R''' and R'''' values are due to that this specimen has the highest fracture toughness (K_{IC}) and the lowest fracture strength (σ_f). As described in Section 3.2, the high K_{IC} value in 1% ZnO added specimen is mainly due to the difficulty of crack propagation leading to shorter crack length in micro-indentation tests, whereas the lowest fracture strength is caused by its lower sintering density.

3.4. Critical quenching temperature

Fig. 2 shows the residual flexural strength as the function of the quenching temperatures. The residual strength behaviors

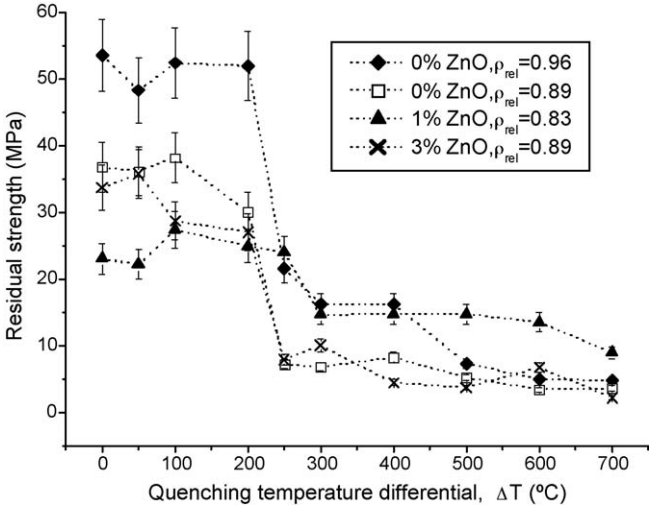

Fig. 2. The residual strength plotted as function of quenching temperatures for specimens with varied relative densities and ZnO concentrations.

follow Hasselman's theory that significant strength degradation appears at a critical thermal shock temperature difference ΔT_c [7].

Two distinct ΔT_c values are observed in four specimens. The specimens of 0% ZnO high density, 0% ZnO low density and 3% ZnO demonstrate acute strength degradation at ΔT_c of approximately 250 °C. The 1% ZnO added sample then shows a higher ΔT_c of 300 °C indicating this specimen has a better thermal shock damage resistance capability. This is consistent with its higher R''' and R'''' values evaluated in Section 3.3.

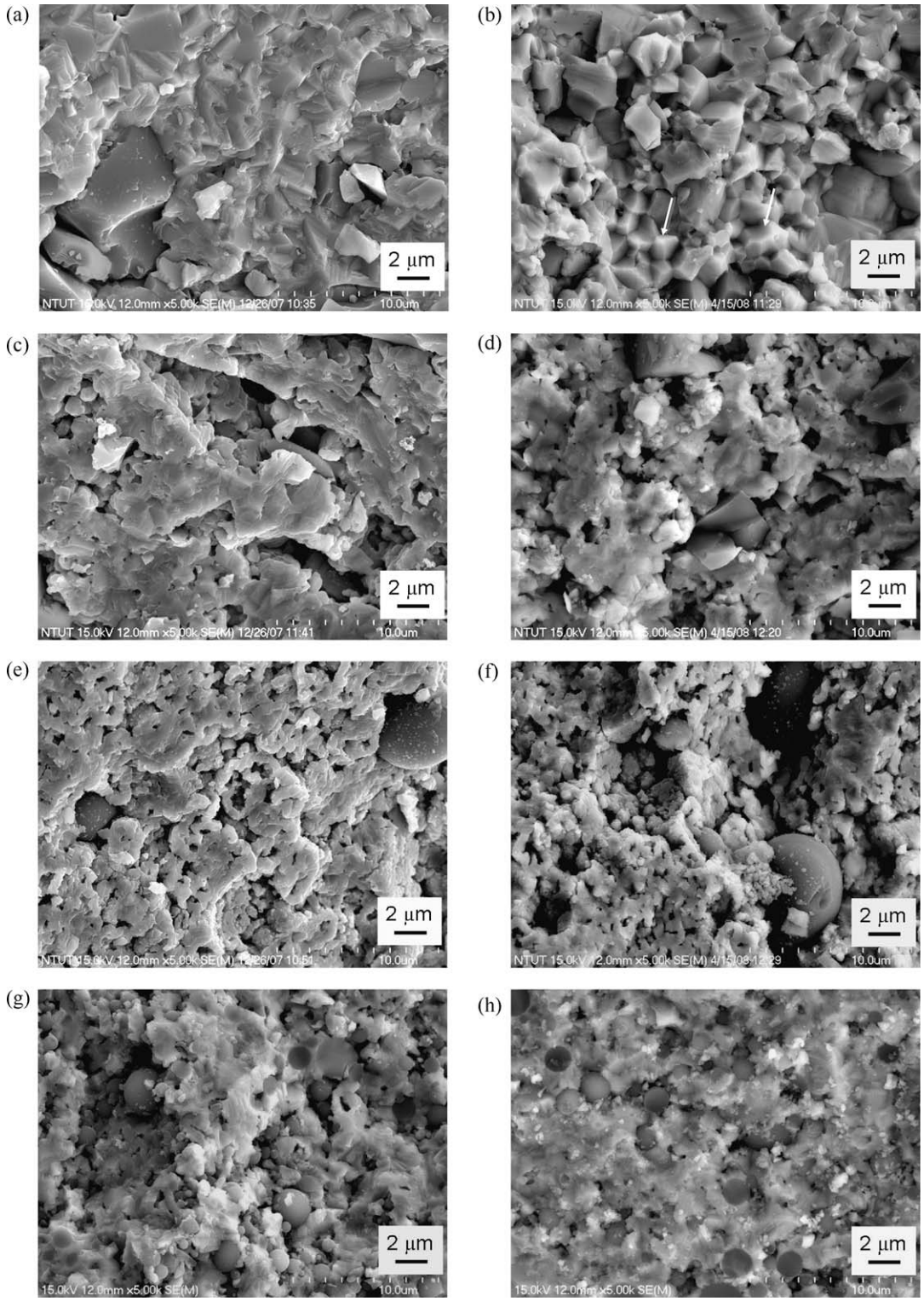

Fig. 3. SEM fractographs of specimens with different ZnO concentration, relative density quenched from two different temperatures: (a) 0% ZnO, $\rho_{rel} = 0.96$, $\Delta T = 0$ °C; (b) 0% ZnO, $\rho_{rel} = 0.96$, $\Delta T = 500$ °C; (c) 0% ZnO, $\rho_{rel} = 0.89$, $\Delta T = 0$ °C; (d) 0% ZnO, $\rho_{rel} = 0.89$, $\Delta T = 500$ °C; (e) 1% ZnO, $\rho_{rel} = 0.83$, $\Delta T = 0$ °C; (f) 1% ZnO, $\rho_{rel} = 0.83$, $\Delta T = 500$ °C; (g) 3% ZnO, $\rho_{rel} = 0.89$, $\Delta T = 0$ °C; (h) 3% ZnO, $\rho_{rel} = 0.89$, $\Delta T = 500$ °C.

In 0% ZnO high density specimen, the flexural strength is higher than the other specimens (Table 1) presumably due to its high sintering density. According to the theory of thermal shock fracture, this specimen is more resistant to crack initiation. However, its ΔT_c is 250 °C which is lower than ΔT_c of 300 °C of 1% ZnO added sample. It confirms that the crack propagation rather than crack initiation dominates thermal shock behaviors in current composite ceramic system.

The residual strength of 0% ZnO high density specimen not only drops greatly at 250 °C temperature difference but also demonstrates another decrease in strength when temperature difference further rises to approximately 500 °C ($\Delta T_c'$). This $\Delta T_c'$ requires additional energy for crack to propagate further and results in another strength degradation [7]. This might be explained by the great difference in coefficients of thermal expansion (CTE) between ZnS (6.36 ppm/°C) and SiO_2 (0.55 ppm/°C) which increase the thermal stresses. This thermal stress effect can become more prominent at higher ΔT when sintering density is high as in the 0% ZnO high density specimen.

On the other hand, formation of willemite ($CTE_{willemite}$ = 1.5 ppm/°C) in ZnO added specimens can act as a buffer at the interface between the ZnS and SiO_2 particles [27]. However, the 3% ZnO added specimen also exhibits poor resistance to thermal shock damage (Table 1). The excessive amount of willemite formed in 3% ZnO added specimen [23] can invertly embrittle the ZnS–SiO_2 interface. This specimen thus has among all the lowest fracture toughness and R'''' value.

From the above discussions, the improved thermal shock resistance is achieved through moderate willemite formation and porosity [25,28]. And these requirements are both met by the 1% ZnO added specimen.

3.5. Fractography observations

Fig. 3 shows the fractographs of all specimens at two different quenching temperature differences, $\Delta T = 0$ °C and $\Delta T = 500$ °C. The fracture surface of 0% ZnO high density specimen change obviously from intragranular fracture at $\Delta T = 0$ °C (Fig. 3(a)) to intergranular fracture at $\Delta T = 500$ °C (Fig. 3(b)). The abrupt change of fracture types represents aggravated damages as reported by Li and Ma [29] and You et al. [30]. Therefore, the 0% ZnO high density specimen demonstrates the lowest thermal shock damage parameters and a second ΔT_c at 500 °C.

The fractographs of 0% ZnO low density specimen (Fig. 3(c) and (d)) and 3% ZnO added specimen (Fig. 3(g) and (h)) remain the intragranular fracture type at both $\Delta T = 0$ °C and $\Delta T = 500$ °C. Although the fracture type in these specimens does not change as drastic as those shown in the 0% ZnO high density specimen (Fig. 3(a) and (b)), flatter and large size cleavages extend over the entire fracture surfaces in Fig. 3(d) and (h). It indicates that the cracks propagate fairly easy across the specimens without crack deflections. In 0% ZnO low density specimen, the cracks penetrate the SiO_2 particles at $\Delta T = 500$ °C (Fig. 3(d)) without appreciable resistance. In 3% ZnO added specimen, on the other hand, the fractograph of $\Delta T = 500$ °C (Fig. 3(h)) shows many fragile residues on fracture surface. This demonstrates the embrittlement caused by excess willemite formation at ZnS and SiO_2 interfaces which leads to cleavages in SiO_2 particles. Therefore, both of these specimens give rise to flat fracture surfaces and great drops in their residual strengths.

In 1% ZnO added specimen, the fracture types at $\Delta T = 0$ °C and at $\Delta T = 500$ °C do not differ much (Fig. 3(e) and (f)). Fractures travel along the ZnS–SiO_2 interfaces and pores. The ZnS–SiO_2 interfaces and pores appear to assist in deflecting and arresting the cracks. Thin layer of willemite at SiO_2 surfaces acts as a buffer to reduce thermal stress between ZnS and SiO_2 and avoid cleavages of SiO_2 particles (Fig. 3(f)) in contrast to those shown in Fig. 3(d) and (h). Therefore the residual strength is the highest among the four specimens at high quenching temperatures. These observations again correspond well with the higher thermal shock parameters given by the 1% ZnO added specimen.

4. Conclusions

Thermal shock behavior of hot pressed ZnO–ZnS–SiO_2 composite ceramics is studied by water quenching method. The ZnO addition does not improve the sintering density but forms willemite by reacting SiO_2 and ZnO. Higher sintering density and excessive willemite formation can both embrittle the microstructures and cause the fracture toughness and the thermal shock damage parameters to drop. The highest values of R''' and R'''' are obtained by 1% ZnO added specimen. The improved thermal shock resistance is attributed to increased fracture toughness by moderate ZnO addition and porosity. Thin layer of willemite can act as a buffer layer to protect SiO_2 particles from been cleaved, while moderate amount of pores assist in arresting the cracks. The calculated thermal shock damage parameters are shown to correspond well with the observations made in ZnO–ZnS–SiO_2 composite ceramic system.

Acknowledgements

The authors would like to express their appreciation for financial support of China Steel Corporation under grant #RE95002 and National Science Council of Taiwan under grant NSC-96-2622-E-027-001-CC3.

References

[1] W.C. Lin, T.S. Kao, H.H. Chang, Y.H. Lin, Y.H. Fu, C.T. Wu, K.H. Chen, D.P. Tsai, Study of a super-resolution optical structure: polycarbonate/ZnS–SiO_2/ZnO/ZnS–SiO_2/$Ge_2Sb_2Te_5$/ZnS–SiO_2, Japanese Journal of Applied Physics 42 (2003) 1029–1030.
[2] M. Horie, T. Ohno, Durability of dielectric protective layers against repetitious thermal stress in phase-change optical recording, Thin Solid Films 278 (1–2) (1996) 74–81.
[3] D.V. Tsu, T. Ohta, Mechanism of properties of noble ZnS–SiO_2 protection layer for phase change optical disc media, Japanese Journal of Applied Physics 45 (2006) 6294–6307.
[4] E.H. Lutz, M.V. Swain, N. Claussen, Thermal shock behavior of duplex ceramics, Journal of the American Ceramic Society 74 (1) (1991) 19–24.

[5] D.P.H. Hasselman, Thermal shock by radiation heating, Journal of the American Ceramic Society 46 (5) (1963) 229–234.
[6] D.P.H. Hasselman, Theory of Thermal shock resistance of semitransparent ceramics under radiation heating, Journal of the American Ceramic Society 49 (2) (1965) 103–104.
[7] D.P.H. Hasselman, Unified Theory of thermal shock fracture initiation and crack propagation in brittle ceramics, Journal of the American Ceramic Society 52 (11) (1969) 600–604.
[8] D.P.H. Hasselman, Thermal stress resistance parameters for brittle refractory ceramics: a compendium, Ceramic Bulletin 49 (12) (1970) 1033–1037.
[9] W.D. Kingery, Factors affecting thermal stress resistance of ceramic materials, Journal of the American Ceramic Society 38 (1) (1954) 3–15.
[10] C. Aksel, P.D. Warren, Thermal shock parameters [R, R''' and R''''] of magnesia-spinel composite, Journal of the European Ceramic Society 23 (2003) 301–308.
[11] Z. Zhou, P. Ding, S. Tan, J. Lan, A new thermal-shock-resistance model for ceramics: establishment and validation, Materials Science and Engineering A 405 (2005) 272–276.
[12] M. Aldridge, J.A. Yeomans, The thermal shock behavior of dutile particle toughed alumina composites, Journal of the European Ceramic Society 19 (1998) 1769–1775.
[13] D.R. Lide, CRC Handbook of Chemistry and Physics, 85th ed., CRC Press, New York, 2004.
[14] ASTM, Standard Test Method for Determination of Thermal Shock Resistance for Advanced Ceramics by Water Quenching, Designation: C 1525-04.
[15] P. Chantikul, G.R. Anstis, B.R. Lawn, D.B. Marshall, A critical evaluation of indentation techniques for measuring fracture toughness: II, strength method, Journal of the American Ceramic Society 64 (9) (1981) 539–543.
[16] Z. Li, A. Ghosh, A.S. Kobayashi, R.C. Bradt, Indentation fracture toughness of sintered silicon carbide in the palmqvist crack regime, Journal of the American Ceramic Society 72 (6) (1989) 904–911.
[17] G.R. Anstis, P. Chantikul, B.R. Lawn, D.B. Marshall, A critical evaluation of indentation techniques for measuring fracture toughness: I, direct crack measurement, Journal of the American Ceramic Society 64 (9) (1981) 533–538.
[18] K. Nihara, A. Nakahira, T. Hirai, The effect of stoichiometry on mechanical properties of boron carbide, Journal of the American Ceramic Society 67 (1) (1984) c13–c14.
[19] G.S. Brady, H.R. Clauster, J.A. Vaccari, Materials Handbook, McGraw-Hill, New York, 2002.
[20] F. Cardarelli, Materials Handbook, Springer, London, 2000.
[21] E.N. Bunting, Phase Equilibrium in the System SiO_2–ZnO, Journal of the American Ceramic Society 13 (1930) 5–10.
[22] Y.B. Chen, C.L. Huang, S.H. Lin, Influence of ZnO additions to $0.8(Mg_{0.95}Co_{0.05})TiO_{3-0.2}Ca_{0.6}La_{0.8}/3TiO_3$ ceramics on sintering behavior and microwave dielectric properties, Materials Letters 60 (2006) 3591–3595.
[23] J.K. Chen, K.L. Tang, T.P. Tang, J.T. Chang, Effects of zinc oxide and porosity on permittivity of sintered zinc sulfide–silicon dioxide, Japanese Journal of Applied Physics 47 (7) (2008) 5539–5544.
[24] J. Merikhi, C. Feldman, Adhesion of colloidal SiO_2 particle on ZnS-type phosphor surfaces, Journal of Colloid and Interface Science 228 (2000) 121–126.
[25] S. Ding, Y.P. Zeng, D. Jiang, Thermal shock behaviour of mullite-bonded porous silicon carbide ceramics with yttria addition, Journal of Physics D: Applied Physics 40 (2007) 2138–2142.
[26] J.N. Shive, The Properties, Physics, and Design of Semiconductor Devices, The Bell Telephone Laboraties Series, D.Van Nostrand Co., New York, 1959.
[27] A.M. Hu, M. Li, D.L. Mao, K.M. Liang, Crstallization and properties of a spodumene-willemite glass ceramic, Thermochimica Acta 437 (2005) 110–113.
[28] V.D. Krstic, Effect of microstructure on fracture of brittle materials: unified approach, Theoretical and Applied Fracture Mechanics 45 (2006) 212–226.
[29] J. Li, L.P. Ma, Influence of cobalt phase on mechanical properties and thermal shock performance of Al_2O_3–TiC somposites, Ceramics International 31 (2005) 945–951.
[30] X.Q. You, T.Z. Si, N. Liu, P.P. Ren, Y.D. Xu, J.P. Feng, Effect of grain size on thermal shock resistance of Al_2O_3–TiC ceramics, Ceramics International 31 (2005) 33–38.